Oxygen Electrocatalysis on Epitaxial La[subscript 0.6]Sr[subscript 0.4]CoO[subscript 3-#] Perovskite Thin Films for Solid Oxide Fuel Cells

Citation: Crumlin, E. J., S.-J. Ahn, D. Lee, E. Mutoro, M. D. Biegalski, H. M. Christen, and Y. Shao-Horn. "Oxygen Electrocatalysis on Epitaxial La[subscript 0.6]Sr[subscript 0.4]CoO[subscript 3-δ] Perovskite Thin Films for Solid Oxide Fuel Cells." Journal of the Electrochemical Society 159, no. 7 (2012): F219-F225.© 2012 The Electrochemical Society.

As Published: http://dx.doi.org/10.1149/2.018207jes

Publisher: Electrochemical Society

Persistent URL: http://hdl.handle.net/1721.1/82605

Version: Final published version: final published article, as it appeared in a journal, conference proceedings, or other formally published context

Journal of The Electrochemical Society, **159** (7) F219-F225 (2012)
0013-4651/2012/159(7)/F219/7/$28.00 © The Electrochemical Society

Oxygen Electrocatalysis on Epitaxial $La_{0.6}Sr_{0.4}CoO_{3-\delta}$ Perovskite Thin Films for Solid Oxide Fuel Cells

Ethan J. Crumlin,[a] Sung-Jin Ahn,[a] Dongkyu Lee,[a] Eva Mutoro,[a] Michael D. Biegalski,[b] Hans M. Christen,[b] and Yang Shao-Horn[a,*,z]

[a]*Electrochemical Energy Laboratory, Massachusetts Institute of Technology, Cambridge, Massachusetts 02139, USA*
[b]*Center for Nanophase Materials Sciences, Oak Ridge National Laboratory, Oak Ridge, Tennessee 37831, USA*

Hetero-structured interfaces of oxides, which can exhibit reactivity characteristics remarkably different from bulk oxides, are interesting systems to explore in search of highly active fuel cell catalysts for oxygen electrocatalysis. (001)-oriented $La_{0.6}Sr_{0.4}CoO_{3-\delta}$ ($LSC60\text{-}40_{113}$) thin films having thicknesses from tens to hundreds of nanometers were grown epitaxially on (001)-oriented yttria-stabilized zirconia (YSZ). Atomic force microscopy showed that all the film surfaces were of high quality with average surface roughness approximately one nanometer. The surface oxygen exchange kinetics of these films were determined by electrochemical impedance spectroscopy. While (001)-oriented $LSC60\text{-}40_{113}$ thin films were found to have similar surface oxygen exchange coefficients to $LSC60\text{-}40_{113}$ bulk, surface coverage of (001)-oriented $(La_{0.5}Sr_{0.5})_2CoO_{4\pm\delta}$ (LSC_{214}) on the $LSC60\text{-}40_{113}$ thin films led to significant enhancement in the surface oxygen kinetics up to ~3 orders of magnitude. Interestingly, LSC_{214}-decorated $LSC60\text{-}40_{113}$ films have comparable surface exchange kinetics ($\sim 1 \cdot 10^{-5}$ cm $\cdot$ s^{-1} at 550°C) to similarly prepared LSC_{214}-decorated $La_{0.8}Sr_{0.2}CoO_{3-\delta}$ films. Such high surface oxygen kinetics are among the most active SOFC cathode materials reported to date.
 [DOI: 10.1149/2.018207jes]

Manuscript submitted February 9, 2012; revised manuscript received March 21, 2012. Published July 17, 2012.

The efficiency of solid oxide fuel cells (SOFCs) is limited primarily by the oxygen reduction reaction (ORR) at the cathode, particularly for SOFCs operated at intermediate temperatures. Therefore, there is a need to search for electrode materials with enhanced ORR activity. Mixed electronic and ionic conductors such as ABO_3 perovskites[1–3] and A_2BO_4 Ruddlesden-Popper materials,[4] are promising cathode materials due to their high oxygen ion diffusivity and surface exchange properties. Hetero-structured oxide interfaces have shown surprisingly high oxygen surface exchange properties.[5–11] Recently Sase et al.[9] have reported enhanced ORR kinetics of ~3 orders of magnitude at the interfaces between bulk $La_{0.6}Sr_{0.4}CoO_{3-\delta}$ ($LSC60\text{-}40_{113}$) grains and secondary $(La,Sr)_2CoO_{4\pm\delta}$ precipitates relative to bulk $LSC60\text{-}40_{113}$, having an estimated surface oxygen coefficient approaching $1 \cdot 10^{-5}$ cm $\cdot$ s^{-1} at 500°C. Subsequently these authors show that ~1 order of magnitude enhancement in ORR activity can be obtained for composite cathodes screen-printed with these two oxide materials.[11] More recently, we have reported that surface decoration of $(La_{0.5}Sr_{0.5})_2CoO_{4\pm\delta}$ (LSC_{214}) particles epitaxially grown on the (001)-oriented $La_{0.8}Sr_{0.2}CoO_{3-\delta}$ thin films, which are epitaxially grown on yttria-stabilized zirconia (YSZ), can lead to marked enhancement in the surface oxygen exchange kinetics up to three orders of magnitude relative to bulk,[5] approaching that of the $LSC60\text{-}40_{113}/LSC_{214}$ interfaces of composite ceramics.[9]

In this study, we investigate the surface oxygen exchange kinetics of (001)-oriented $LSC60\text{-}40_{113}$ and LSC_{214}-decorated $LSC60\text{-}40_{113}$ thin films epitaxially grown on YSZ. First, as (001)-oriented $La_{0.8}Sr_{0.2}CoO_{3-\delta}$ ($LSC80\text{-}20_{113}$) thin films have shown enhanced ORR kinetics by one order of magnitude relative to bulk,[12] we are interested in understanding if (001)-oriented $LSC60\text{-}40_{113}$ thin films would also exhibit enhanced surface oxygen kinetics relative to bulk. Polycrystalline $LSC60\text{-}40_{113}$ thin films[13] supported on a sintered $Gd_{0.2}Ce_{0.8}O_2$ (GDC) substrate show comparable surface oxygen exchange coefficients to that of bulk $LSC60\text{-}40_{113}$ pellet.[14] Considering previous studies[15] have shown that X-ray-diffraction-amorphous $LSC60\text{-}40_{113}$ films have enhanced ORR activity than crystalline films supported on YSZ(001), single-crystalline, (001)-oriented $LSC60\text{-}40_{113}$ films might have different surface oxygen kinetics from polycrystalline $LSC60\text{-}40_{113}$ thin films reported previously.[13] Second, although previous work qualitatively confirm the enhancement at the interfaces between polycrystalline $LSC60\text{-}40_{113}$ and $(La,Sr)_2CoO_4$ thin films,[8] we aim to quantify the degree of enhancement in the surface oxygen exchange kinetics associated with LSC_{214} decoration on (001)-oriented $LSC60\text{-}40_{113}$ films. In this study, we report ORR activities for epitaxial (001)-oriented $LSC60\text{-}40_{113}$ films comparable to bulk $LSC60\text{-}40_{113}$. In addition, surface LSC_{214} decoration grown epitaxially on the (001)-oriented $LSC60\text{-}40_{113}$ thin films can provide activity enhancement up to 3 orders of magnitude relative to bulk, and have surface oxygen exchange coefficients comparable to those found for LSC_{214}-decorated $LSC80\text{-}20_{113}$ reported previously.[5]

Experimental

$LSC60\text{-}40_{113}$ powders were synthesized by a solid-state reaction using a stoichiometric mixture of La_2O_3, $SrCO_3$, and Co_3O_4 (Alfa Aesar, USA) 1,000°C in air for 12 hours. LSC_{214} and $Gd_{0.2}Ce_{0.8}O_2$ (GDC) was prepared by the Pechini method using $La(NO_3)_3 \cdot 6H_2O$, $Sr(NO_3)_2$, $Co(NO_3)_2 \cdot 6H_2O$, and $Gd(NO_3)_3$ and $Ce(NO_3)_3$, respectively. The precursors were dissolved in de-ionized water with citric acid, and ethylene glycol (Sigma-Aldrich, USA) mixture. After esterification at 100°C, the resin was charred at 400°C and then calcined at 1000°C in air for 12 hours. Pulsed laser deposition (PLD) targets of $LSC60\text{-}40_{113}$, LSC_{214}, GDC with a diameter of 25 mm were fabricated by uniaxial pressing at 50 MPa and sintering at 1,350°C in air for 20 hours.

Single-crystal 9.5 mol% Y_2O_3-stabilized ZrO_2 (YSZ) substrates with the (001)-orientation and a dimension of 10 × 10 × 0.5 mm (Princeton Scientific, USA, one sided polished) were used for the substrate for film deposition and the electrolyte for activity measurements. Prior to film deposition, platinum ink (Pt) (#6082, BASF, USA) counter electrodes were painted on the unpolished side of the YSZ and sintered at 800°C in air for 1 hour. The YSZ substrate was affixed to the PLD substrate holder using a small amount of silver paint (Leitsilber 200, Ted Pella, USA) for thermal contact. PLD was performed using the following parameters: KrF excimer laser (λ = 248 nm), 10 Hz pulse rate, ≈50 mJ pulse energy, distance between target and substrate ~5 cm, and $p(O_2)$ = 10 mTorr. To prevent the reactivity between YSZ and $LSC60\text{-}40_{113}$, 500 pulses of GDC were deposited first at 450°C (~ 5 nm thick estimated from scanning transmission electron microscopy on similar samples as reported previously,[5] having ~0.01 nm/laser-pulse). This was followed by 5,000, 15,000, or 30,000 pulses of $LSC60\text{-}40_{113}$ (~0.005 nm/laser-pulse) at 675°C to produce films of different thicknesses, which was cooled to room temperature within ~1 h in 10 mTorr $p(O_2)$. LSC_{214}-decorated $LSC60\text{-}40_{113}$ films were fabricated by adding 25, 150, 900, and 2700 pulses on the $LSC60\text{-}40_{113}$ film of 15,000 pulses, which led to surface LSC_{214} decoration thickness of ~0.1 nm (partial coverage), ~0.8 nm, (partial coverage), ~5 nm (likely full coverage) and

*Electrochemical Society Active Member.
zE-mail: shaohorn@mit.edu

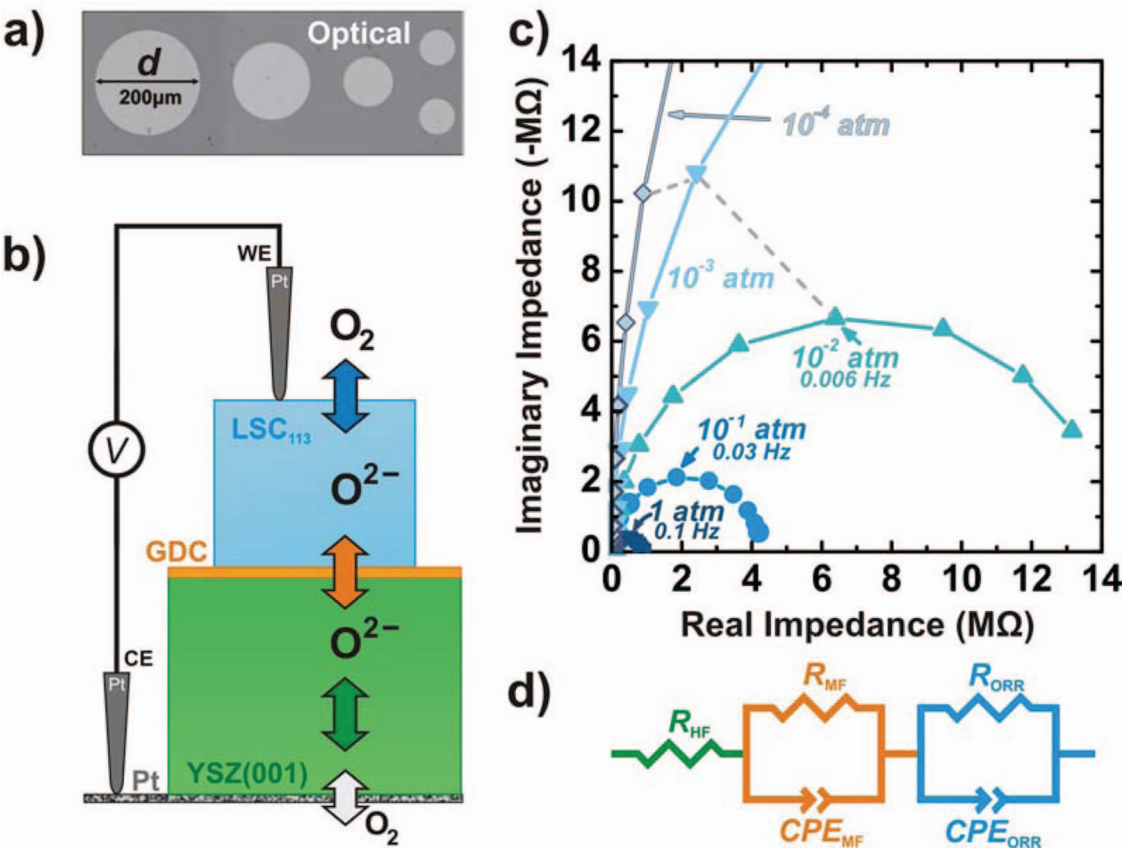

Figure 1. a) Optical images of a LSC60-40$_{113}$(001)/GDC(001)/YSZ(001)/porous Pt sample and the electrochemical testing configuration, b) schematics of LSC microelectrodes on GDC/YSZ, c) characteristic Nyquist plot of a 200 μm-microelectrode at 520°C and varying $p(O_2)$, and d) equivalent circuit (R_{HF} = YSZ electrolyte resistance, R_{MF} = electrode/electrolyte interface resistance, R_{ORR} = ORR resistance, CPE = constant phase element) used to extract ORR kinetics.

~15 nm (full coverage), respectively, a linear thickness extrapolation was based on previous work of LSC$_{214}$ decoration of LSC80-20$_{113}$ films.[5,16] A reference film of LSC60-40$_{113}$ decorated with 25 pulses of LSC60-40$_{113}$ was also fabricated for comparison.

The phase purity of oxide powder samples for PLD targets were investigated via high resolution X-ray diffraction (XRD) using a four-circle diffractometer (Panalytical, USA). Thin film XRD was performed using a four-circle diffractometer (Bruker D8, Germany) in normal and off-normal configurations. Film surface morphologies were examined by optical microscopy (Carl Zeiss, Germany) and atomic force microscopy (AFM) (Veeco, USA).

Micrometer-scale, circular LSC60-40$_{113}$ electrodes with and without LSC$_{214}$-decoration were fabricated by photolithography and the following process: OCG positive photoresist (Arch Chemical Co, USA) was applied on the film surface and patterned using a mask aligner (Karl Süss, Germany, λ = 365 nm). The photoresist was developed using Developer 934 1:1 (Arch Chemical Co., USA) developer, and the films were subsequently etched in hydrochloric acid (HCl) to form circular microelectrodes (diameters of 25 μm – 200 μm as determined by optical microscopy, Figure 1a). The photoresist was removed with acetone. The microelectrode sizes and morphological stability were examined by optical microscopy and AFM before and during electrochemical testing. AFM was then used to measure the LSC60-40$_{113}$ film thickness after microelectrode patterning, which showed thicknesses of 22, 77 and 157 nm for 5,000, 15,000 and 30,000 pulses, respectively. LSC$_{214}$-decorated LSC60-40$_{113}$ films were found to have 88, 85, 88, and 97 nm for LSC$_{214}$ coverage of ~0.1, ~0.8, ~5 and ~15 nm, respectively. The thickness of the reference LSC60-40$_{113}$-covered LSC60-40$_{113}$ was 85 nm.

Electrochemical impedance spectroscopy (EIS) measurements of microelectrodes of ~ 200 μm in diameter, which were contacted by Pt-coated tungsten carbide probes, were performed using a microprobe station (Karl Süss, Germany) connected to a frequency response analyzer (Solartron 1260, USA) and dielectric interface (Solartron 1296, USA), as shown in Figure 1b. The porous Pt counter electrode was placed on a conductive substrate and fixed with Ag paste (Leitsilber 200, Ted Pella, USA). The temperature was controlled at 520°C (for LSC60-40$_{113}$ thin films) and 550°C (for LSC60-40$_{113}$ thin films with LSC$_{214}$ surface decoration) with heating stage (Linkam TS1500, UK) and calibrated using a second thermocouple contacting the thin film surface. Data were collected between 1 MHz and 1 mHz using a voltage amplitude of 10 mV under Ar / O_2 mixtures in the $p(O_2)$ range of $1 \cdot 10^{-4}$ to 1 atm. ZView software (Scribner Associates, USA) was used to analyze the EIS data. Multiple electrodes (at least three) of all films were measured by EIS at each temperature and $p(O_2)$ to ensure that the EIS results were reproducible and representative. The high-frenquency intercept corresponds to the oxygen ion conduction resistance in YSZ and the mid-frequency feature is believed to result from the interface between YSZ and GDC as reported previously.[5]

The film thicknesses of LSC60-40$_{113}$ films are considerably smaller than the critical thickness, t_{crit}, of ≈ 20 μm found for bulk LSC60-40$_{113}$ at 518°C and $p(O_2)$ = 0.23 bar.[14] t_{crit} is defined as D^*/k^*, where D^* is the tracer oxygen diffusivity and k^* the tracer surface exchange coefficient,[17] below which surface oxygen exchange limits the ORR kinetics. Therefore, the ORR kinetics of these films were governed primarily by surface oxygen exchange kinetics. With this understanding, the EIS data (Figure 1c) were analyzed using a simplified equivalent circuit shown in Figure 1d, from which the ORR resistance (R_{ORR}) and oxygen surface exchange coefficients were obtained as follows. The extracted low-frequency resistance values (R_{LF} = R_{ORR}) were used to calculate the surface exchange

coefficients k^q by:[5,12,18]

$$k^q = \frac{RT}{4F^2 R_{ORR} A_{electrode} c_0} \quad (1)$$

where R is the universal gas constant (8.314 J $mol^{-1} \cdot K^{-1}$), T is the absolute temperature (793 K), F is the Faraday's constant (96,500 $C \cdot mol^{-1}$), $A_{electrode}$ is the area of the microelectrode, and c_0 is the lattice oxygen concentration in LSC.

Results and Discussion

Normal X-ray diffraction (XRD) data (Figure 2a) clearly show the presence of the $(00l)_{pc}$ of $LSC60\text{-}40_{113}$ and the $(00l)_{cubic}$ (l is even) peaks of GDC, and YSZ, which indicates $(001)_{pc}LSC60\text{-}40_{113}$ // $(001)_{cubic}GDC$ // $(001)_{cubic}YSZ$. The subscript "pc" denotes the pseudocubic notation, where the rhombohedral structure of $LSC60\text{-}40_{113}$ bulk is approximated with an average for all film thicknesses of $\boldsymbol{a}_{pc} \approx 3.847$ Å (Table I).[5,12] With LSC_{214} coverage equal to or greater than ~5 nm in thickness, the $(00l)_{tetragonal}$ peaks (l is even) of LSC_{214} become visible (Figure 2b), which indicates $(001)_{tetragonal}LSC_{214}$ // $(001)_{pc}LSC60\text{-}40_{113}$ // $(001)_{cubic}GDC$ // $(001)_{cubic}YSZ$. These peaks give rise to $\boldsymbol{c}_{tetragonal} = 12.5$ Å for LSC_{214}, which is comparable to previously reported values.[19,20] Off-normal phi-scan analysis shows that $LSC60\text{-}40_{113}\{101\}_{pc}$, $GDC\{202\}_{cubic}$ and $YSZ\{202\}_{cubic}$ have strong peaks with 4-fold cubic symmetry (Figure S1a),[21] which reveals the in-plane crystallographic relationships between GDC and YSZ (a cube-on-cube alignment), and $LSC60\text{-}40_{113}$ and GDC (a in-plane 45° rotation), having $[100]_{pc}LSC60\text{-}40_{113}$//$[110]_{cubic}GDC$//$[110]_{cubic}YSZ$ (Figure S1b).[21] These results are in agreement with our previously published findings for $LSC80\text{-}20_{113}$ thin films.[5,12] The in-plane crystallographic relationship between $LSC60\text{-}40_{113}$ and LSC_{214} was not independently measured but it is likely to have $[100]_{pc}LSC60\text{-}40_{113}$ // $[100]_{tetragonal}LSC_{214}$ as shown previously for LSC_{214} decoration on (001)-oriented $LSC80\text{-}20_{113}$.[5]

$LSC60\text{-}40_{113}$ films were found dilated in-plane and compressed in the direction normal to the film surface at room temperature with good crystallinity (Table I and Figure S2[21]). It is interesting to note that the in-plane and normal strains decrease with increasing film thickness from 25 to 157 nm. The origin of these strains might be a consequence of different thermal expansion coefficients between YSZ (~11×10^{-6}°C^{-1})[22] and $LSC60\text{-}40_{113}$ films (~15.8×10^{-6}°C^{-1} for bulk[23]). Experiments are ongoing to examine how these strains change upon heating to high temperatures. Of significance to note is that the $LSC60\text{-}40_{113}$ films have slightly smaller relaxed lattice parameters than bulk (3.855 Å[24]) at room temperature. The relaxed lattice parameter, $\hat{\boldsymbol{a}}_{pc}$, can be estimated by assuming a Poisson ratio of 0.25[25] for $LSC60\text{-}40_{113}$, which gives rise to $\hat{\boldsymbol{a}}_{pc} = 3.847$ Å, 3.849 Å and 3.845 Å for the films of 25, 77 and 157 nm, respectively. Having different relaxed unit cell volume from bulk materials is commonly noted for PLD films, which may result from different oxygen nonstoichiometry[12,23,25] and/or microstructure.[12,26] Unlike (001)-oriented epitaxial $LSC80\text{-}20_{113}$ films that have larger relaxed lattice parameter than bulk,[5,12] (001)-oriented epitaxial $LSC60\text{-}40_{113}$

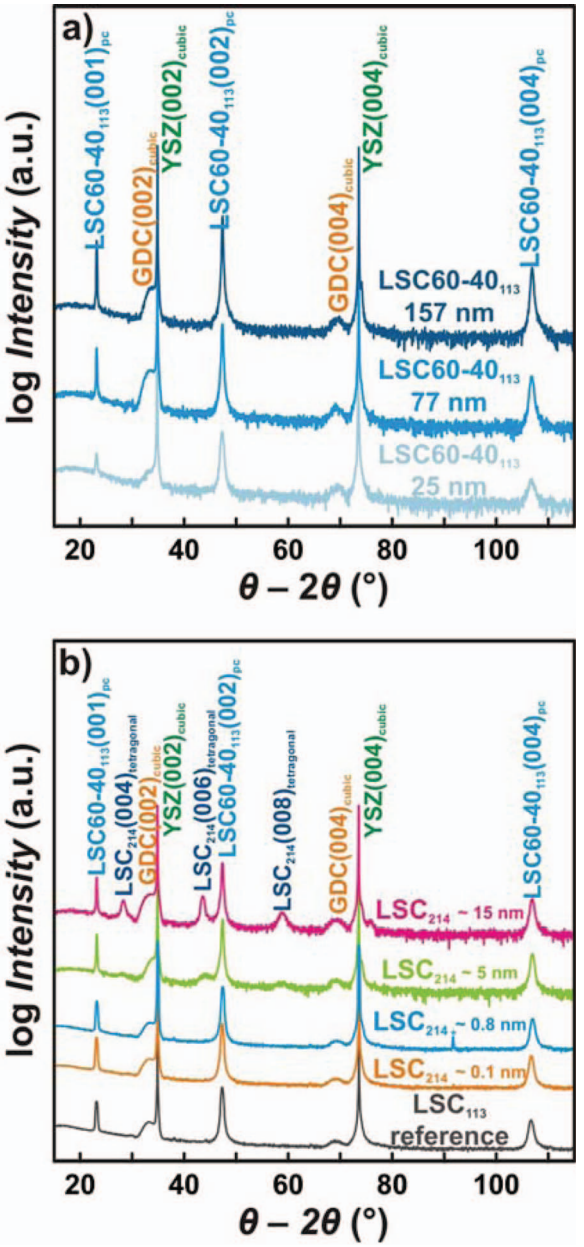

Figure 2. Normal XRD data of a) $LSC60\text{-}40_{113}$ films of 25, 77 and 157 nm on $GDC(001)_{cubic}/YSZ\ (001)_{cubic}$ substrate, b) $LSC60\text{-}40_{113}$ reference and LSC_{214}-decorated ~85 nm thick $LSC60\text{-}40_{113}$ films. The (*) denotes a singular unknown artifact peak for the ~0.8 nm LSC_{214} surface decorated film.

Table I. Constrained and relaxed lattice parameters of $LSC60\text{-}40_{113}$ films extracted from normal and off-normal XRD data from 100 mm^2 samples. Constrained normal and in-plane lattice parameters of $LSC60\text{-}40_{113}$ films were calculated from combining the inter-planar distance of the $(002)_{pc}$ and $(101)_{pc}$ peaks. For reference lattice parameter and strain values for $LSC80\text{-}20_{113}$ films is provided in Table S1.[12,21]

Materials	Constrained in-plane a (Å)	Constrained normal c (Å)	Relaxed film lattice parameter[a] $\hat{a}$ (Å)	In-plane strain $\varepsilon_{xx} = \frac{(a-\hat{a})}{\hat{a}}$	Normal strain $\varepsilon_{zz} = \frac{(c-\hat{a})}{\hat{a}}$
$LSC60\text{-}40_{113\text{-}25\ nm}$ (pc)	3.870	3.831	3.847	0.60%	−0.40%
$LSC60\text{-}40_{113\text{-}77\ nm}$ (pc)	3.870	3.836	3.849	0.53%	−0.35%
$LSC60\text{-}40_{113\text{-}157\ nm}$ (pc)	3.860	3.834	3.845	0.41%	−0.27%

[a] $\hat{a}$ was calculated from $\frac{\Delta c}{\hat{c}} = \frac{-2\nu}{1-\nu}\frac{\Delta a}{\hat{a}}$, assuming $\hat{a} = \hat{c}$ and $\nu = 0.25$ for $LSC60\text{-}40_{113}$.

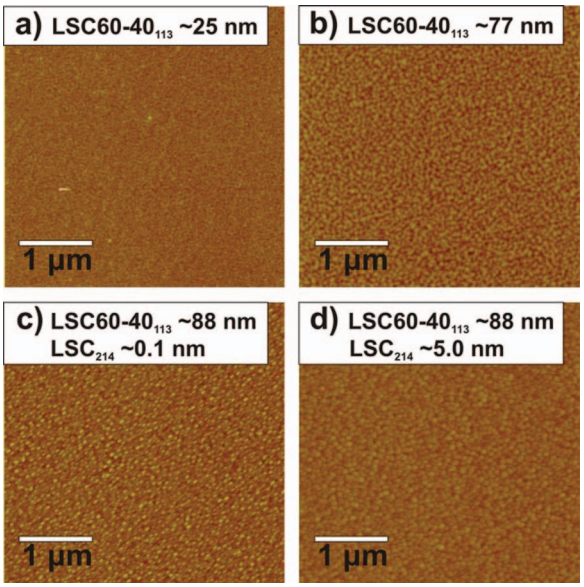

Figure 3. AFM measurements of a) LSC60-40_{113} ~ 25 nm with RMS of 0.8 nm b) LSC60-40_{113} ~ 77 nm with RMS of 0.8 nm, c) LSC60-40_{113} ~ 88 nm with LSC_{214} ~0.1 nm with RMS of 1.1 nm, and d) LSC60-40_{113} ~ 88 nm with LSC_{214} ~5 nm with RMS of 0.6 nm. AFM images are shown with maximum height of 20 nm.

films were found to have smaller relaxed lattice parameters than bulk, which is indicative of lower oxygen vacancies in the films.

AFM imaging revealed that the surface roughness of as-deposited LSC60-40_{113} films have low root-mean-squared (RMS) roughness less than ~1 nm (Figures 3 and S3[21]). AFM images of LSC60-40_{113} of 25 nm, 77 nm, LSC_{214}-decorated 0.1 nm and 5.0 nm are shown in Figure 3, and AFM images of remaining films are shown in Figure S3.[21] With LSC_{214} coverage on LSC60-40_{113} films, there was no significant change in the surface roughness. The surface roughness of these LSC60-40_{113} and LSC_{214}-decorated LSC60-40_{113} films are comparable to those of LSC80-20_{113} and LSC_{214}-decorated LSC80-20_{113} films, respectively.[5]

EIS data of all LSC60-40_{113} thin films were found to be very similar in shape, and typical features in the Nyquist plots are shown in the schematic in Figures 1c and S4.[21] The predominant semicircle (assigned to the impedance of surface oxygen exchange kinetics) was found to increase with decreasing $p(O_2)$. The electrical surface exchange coefficient, k^q, was extracted from the real impedance while chemical surface exchange coefficient, k_{chem}, which describes the rate of surface oxygen exchange with chemical driving force, was estimated from the semicircle peak frequency (Supplementary Information[21]). The electrical surface exchange (k^q) and chemical surface exchange (k_{chem}) coefficients of LSC60-40_{113} films of different thicknesses at 520°C are plotted as a function of oxygen partial pressure, $p(O_2)$ in Figures 4a and 4b, respectively. All LSC60-40_{113} films exhibited comparable k^q and k_{chem}, which appeared to be thickness independent. It is interesting to note that the strains in LSC60-40_{113} thin films measured at room temperature do not appear to correlate with surface oxygen exchange coefficients (Figure S5).[21] Assuming k^q can be approximated as k^*,[27] these k^q and k_{chem} values of the LSC60-40_{113} thin films are comparable to those extrapolated for bulk LSC60-40_{113},[9,14] as shown in Figure 4. It should be mentioned that the (001)-oriented epitaxial LSC60-40_{113} films in this study have comparable surface oxygen coefficients ($\sim 3\times10^{-8}$ cm · s^{-1} at 0.1 atm) than those from polycrystalline LSC60-40_{113} films extrapolated to 520°C at $p(O_2)$ of 0.1 atm or lower.

LSC_{214} surface decoration on LSC60-40_{113} films led to markedly smaller real impedance and much greater surface oxygen exchange kinetics relative to LSC60-40_{113} and the LSC60-40_{113}-covered reference film (Figure S6).[21] At $p(O_2)$ of $1\cdot10^{-4}$ and $1\cdot10^{-2}$ atm, LSC_{214}-decoration increased k^q up to ~2 orders of magnitude relative to the reference LSC60-40_{113} film, having low coverage of 0.1 and 0.8 nm exhibiting the highest k^q values, as shown in Figure 5a. At $p(O_2)$ greater than 10^{-2} atm, the enhancement with surface coverage was ~1 order of magnitude. At these high $p(O_2)$ conditions, the very high k^q values ($\sim1\cdot10^{-6}$ cm · s^{-1} or higher) can decrease the critical thickness assuming a constant diffusion coefficient, and thus lead to ORR impedance to be influenced by bulk oxygen ion diffusion in addition to surface oxygen exchange. The much decreased $p(O_2)$ dependency of k^q for LSC_{214}-decorated LSC60-40_{113} films with low coverage at these high $p(O_2)$ further supports that ORR kinetics are limited also by bulk oxygen ion diffusion in the films of ~90 nm as typically oxygen ion diffusion is inversely proportional to $p(O_2)$.[14] Therefore, EIS measurements in the low $p(O_2)$ range from $1\cdot10^{-4}$ to $1\cdot10^{-2}$ atm better reflect the enhancement in the surface exchange kinetics associated with LSC_{214}-decoration. The k^q values of LSC_{214}-decorated LSC60-40_{113} films (0.1 nm) obtained from this study is ~2–3 orders of magnitude higher than that of bulk LSC60-40_{113}.[9,14] Interestingly, the LSC_{214}-decorated LSC60-40_{113} films have comparable surface exchange coefficients to that estimated for the interfaces between bulk $La_{0.6}Sr_{0.4}CoO_{3-\delta}$ (LSC60-40_{113}) grains and secondary $(La,Sr)_2CoO_4$ precipitates relative at 500°C and 0.2 atm.[9] Such high surface oxygen kinetics is comparable to those of the most active

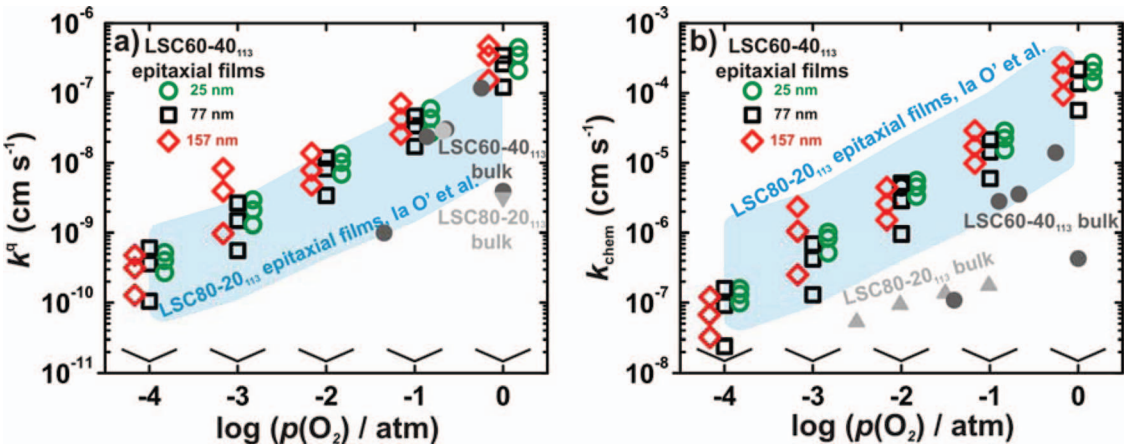

Figure 4. a) k^q and b) k_{chem} from LSC60-40_{113} microelectrodes of 25, 77 and 157 nm calculated from EIS spectra collected at 520°C. Extrapolated bulk k^* (approximately equivalent to k^q)[26] values obtained from previous data of (●-light gray) Sase et al.,[9] (●-dark gray) Berenov et al.,[14] (▼-light gray) De Souza et al.,[32] (▲-light gray) van der Haar et al.[31] are plotted for comparison. Blue shaded regions are the range of k^q and k_{chem} obtained from LSC80-20_{113} film (film thicknesses of 20 nm to 130 nm).[12]

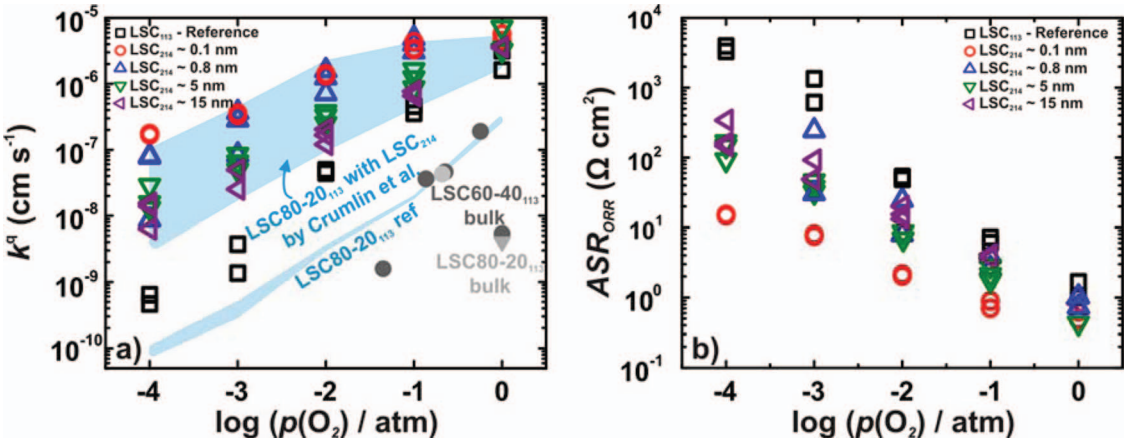

Figure 5. a) Oxygen partial pressure dependency of the surface exchange coefficients, k^q, and b) area specific resistances of the LSC60-40_{113} films with LSC_{214} surface coverage of ~0.1, ~0.8, ~5 and ~15 nm and the LSC60-40_{113}-reference at 550°C. Extrapolated bulk k^* (approximately equivalent to k^q)[26] values obtained from previous studies of (●-light gray) Sase et al.,[9] (●-dark gray) Berenov et al.,[14] (▼-light gray) De Souza et al.[32] are plotted for comparison. Blue shaded region are the range of k^q values obtained from LSC_{214}-decorated LSC80-20_{113} films (LSC_{214} decoration thicknesses of ~0.1 nm to ~15 nm).[5]

cathode materials such as thin-film $Ba_{0.5}Sr_{0.5}Co_{0.8}Fe_{0.2}CoO_{3-\delta}$ [$k^* = \sim 1 \cdot 10^{-6}$ cm · s^{-1} at 500°C and 0.5 bar of $p(O_2)$[28]] and bulk La_2CoO_4 [$k^* = \sim 3 \cdot 10^{-6}$ cm · s^{-1} at 500°C and 0.2 bar of $p(O_2)$[29]]. Moreover, the ORR area specific resistance ($R_{ORR} \cdot Area_{electrode}$) of these LSC_{214}-decorated LSC60-40_{113} films (Figure 5b) at 550°C and are smaller than 1 Ωcm^2 at 0.1 atm and greater, which are among the lowest reported to date.[30]

The $p(O_2)$ dependency of k ($k \propto P_{O_2}^m$) can be indicative of the rate-limiting step of ORR.[31] The $p(O_2)$ dependency of k^q for the LSC60-40_{113} films of different thicknesses was found comparable, having $m_{25nm} = 0.72$, $m_{77nm} = 0.69$, and $m_{157nm} = 0.76$. Similar values were found for k_{chem}: $m_{25nm} = 0.80$, $m_{77\,nm} = 0.78$, and $m_{157nm} = 0.85$. The obtained dependencies for k^q are in good agreement with those reported for bulk $La_{0.3}Sr_{0.7}CoO_{3-\delta}$ and $La_{0.5}Sr_{0.5}CoO_{3-\delta}$.[32] Interestingly, the $p(O_2)$ dependencies of k^q for the LSC_{214}-decorated LSC60-40_{113} films in the range from $1 \cdot 10^{-4}$ to $1 \cdot 10^{-2}$ atm, having $m_{0.1nm} = 0.42$, $m_{0.8nm} = 0.60$, $m_{5.0nm} = 0.61$, and $m_{15.0nm} = 0.53$, are lower than the LSC60-40_{113} films and reference sample ($m_{ref} = 0.90$). It should also be mentioned that these $p(O_2)$ dependencies are lower than that of LSC_{214}-decorated LSC80-20_{113} ($m \sim 0.90$) reported previously.[5] Following the work of Adler et al.,[2] such $p(O_2)$ dependencies suggest that the ORR rate-limiting step for LSC60-40_{113} is dissociative adsorption (m between 0.43 and 0.92).

The k^q and k_{chem} values of (001)-oriented epitaxial LSC60-40_{113} films in this study are comparable to those of (001)-oriented epitaxial LSC80-20_{113} thin films reported previously[5,12] (the range of max. and min. k^q and k_{chem} values shaded in blue in Figure 4), where LSC60-40_{113} have activities toward the upper end of the activity spread of LSC80-20_{113} films. This is in contrast to the fact that bulk LSC60-40_{113}[9,14] has surface exchange coefficients significantly higher than LSC80-20_{113}.[33,34] The enhancement associated with LSC_{214} decoration for LSC60-40_{113} is similar to that reported for LSC80-20_{113} coated with LSC_{214},[5,12] where LSC_{214}-decorated LSC60-40_{113} and LSC80-20_{113} surface have very comparable surface oxygen exchange kinetics (having similar k^q and k_{chem} values in Figure 5a).

We further show that LSC_{214} decoration does not greatly influence the oxygen nonstoichiometry (δ) in the LSC60-40_{113} films, which strongly depends on the La/Sr ratio in the perovskite structure. The oxygen nonstoichiometry (δ) in the LSC60-40_{113} films at 520°C was estimated using volume-specific capacitance (*VSC*). *VSC*s, indicative of changes in the oxygen nonstoichiometry induced by changes in the electrical potential, were extracted from EIS data (Supporting Information).[21] LSC60-40_{113} films of different thicknesses at 520°C had comparable *VSC*s (Figure 6a), which were smaller those of bulk LSC60-40_{113} extrapolated from thermodynamic parameters.[35] We can exclude the contribution of the interfacial capacitance[36] to the *VSC*s

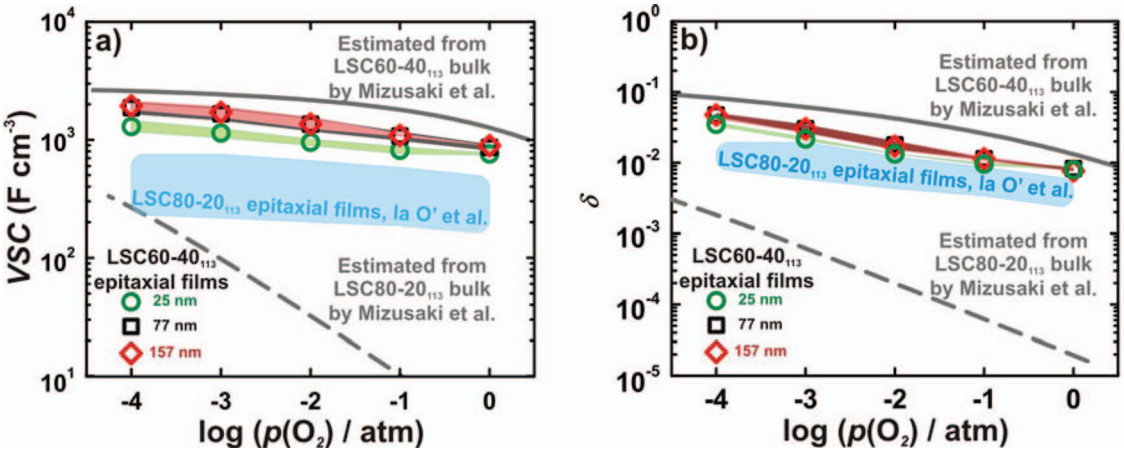

Figure 6. Oxygen partial pressure dependency of a) volume specific capacitance (*VSC*), b) oxygen nonstoichiometry δ of LSC60-40_{113} of 25, 77, and 157 nm at 520°C. Blue shaded regions are the range of *VSC* and δ from LSC80-20_{113}.[12] Values of bulk LSC60-40_{113}[34,36] and LSC80-20_{113}[36] were calculated by using a method reported by Kawada et al.[34]

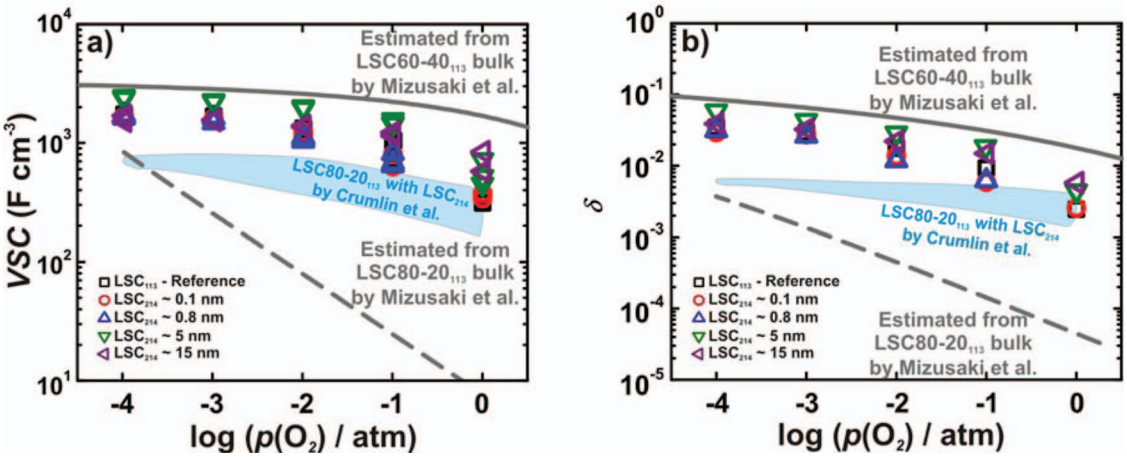

Figure 7. Oxygen partial pressure dependency of a) volume specific capacitance (VSC), b) average oxygen nonstoichiometry δ of LSC60-40_{113}-reference and the ~82 nm LSC60-40_{113} films with ~0.1 nm, ~0.8 nm, ~5 nm, and ~15 nm LSC_{214} surface coverage at 550°C. Blue shaded regions are the range of *VSC* and δ from LSC80-20_{113} with LSC_{214} decoration.[5] Values of bulk LSC60-40_{113}[34,36] and LSC80-20_{113}[36] were calculated by using a method reported by Kawada et al.[34]

of LSC60-40_{113} films as plotting the area specific capacitance (*ASC*) obtained from EIS data as a function of film thickness in Figure S7 yields zero intercept in *ASC*. Correspondingly, oxygen nonstiochiometry, δ, of the LSC60-40_{113} films, which was calculated from the thermodynamic parameters (Table S2)[21] of oxygen vacancy formation in the films based on the $p(O_2)$ dependency of *VSC*, was slightly smaller than that estimated for LSC60-40_{113} bulk,[37] and was similar to that of polycrystalline LSC60-40_{113} films reported by Kawada et al.[35] The lower oxygen nonstoichiometry of LSC60-40_{113} films at 520°C is consistent with smaller relaxed unit cells of LSC60-40_{113} films than bulk LSC60-40_{113} at room temperature (Table I). The (001)-oriented epitaxial LSC60-40_{113} films of this study had higher oxygen nonstiochiometry than similarly prepared LSC80-20_{113} films but the strong influence of the La/Sr ratio albeit its influence on the oxygen nonstiochiometry was found much smaller for thin films than bulk powder samples. As expected, LSC_{214} surface decoration does not appear to influence the oxygen nonstiochiometry of LSC60-40_{113} films, where LSC_{214}-decorated LSC60-40_{113} films had similar oxygen nonstoichiometry and *VSC*s (Figure 7a) to those without decoration.

The thermodynamic enhancement factor (scaling factor between k_{chem} and k^q, and can be related to the density of states near the Fermi Level)[38–40] was determined from k_{chem}/k^q (Figure S8).[21] The thermodynamic enhancement factors of these LSC60-40_{113} films are much higher than that for bulk LSC60-40_{113} reported previously,[37] indicating that it is more difficult to incorporate oxygen ions into the perovskite structure of the films. Similar observations have been made for polycrystalline LSC60-40_{113} films[35] and nanocrystalline LSC50-50_{113} films.[41] Interestingly, the thermodynamic enhancement factor appears to increase with the magnitude of in-plane and normal strains of LSC60-40_{113} films measured at room temperature (Figure S9).[21] Increased thermodynamic enhancement factor can be related to decreased density of states near the Fermi Level of LSC films,[38–40] which requires further studies. This is in contrast to the lack of measurable influence of strains in the LSC60-40_{113} films at room temperature on the surface exchange kinetics (Figures 4 and S5[21]). Moreover, the decoration of LSC_{214} on the surface of LSC60-40_{113} films[8,35] (similar to LSC80-20_{113} films[5]), which greatly enhances the surface exchange kinetics, does not appear to considerably change the thermodynamic non-ideality factor (Table S2),[21] which is in agreement with the hypothesis that LSC_{214} decoration does not significantly alter the thermodynamics of the entire film.

LSC60-40_{113} films showed comparable surface oxygen exchange kinetics and oxygen nonstoichiometry to LSC60-40_{113} bulk, as shown in Figures 6b and 7b. This is in contrast to previous findings of LSC80-20_{113} films,[5,12] which showed much enhanced surface oxygen exchange kinetics (k^q) coupled with higher oxygen nonstoichiometry than LSC80-20_{113} bulk (blue shaded regions). Interestingly, LSC60-40_{113} and LSC80-20_{113} films can have very comparable surface oxygen exchange coefficients (Figures 4a and 4b) but they have considerably dissimilar oxygen stoichiometry.[35,37] These observations suggest that oxygen nonstoichiometry in the films might not control the surface oxygen exchange kinetics, unlike the e_g filling of surface transition metal ions that govern the ORR and OER activities on perovskites in basic solutions over several orders of magnitude.[42,43] This hypothesis does not preclude the possibility that a certain amount of oxygen nonstoichiometry is necessary for high surface oxygen exchange kinetics, and further increase in δ might not lead to activity enhancement. It should be cautioned, however, that oxygen nonstoichiometry shown in Figures 6b and 7b represents the bulk film values, which can be considerably different from that on the surface.

Conclusions

We show that the surface oxygen exchange kinetics and oxygen nonstoichiometry of (001)-oriented LSC60-40_{113} films grown epitaxially on YSZ are comparable to those of LSC60-40_{113} bulk.[13,14] This is in contrast to (001)-oriented LSC80-20_{113} films with enhanced activities and oxygen nonstoichiometry relative to LSC80-20_{113} bulk[32,33] reported previously.[12] In addition, (001)-oriented epitaxial LSC60-40_{113} films have similar surface oxygen exchange coefficient to polycrystalline LSC60-40_{113} films[13] reported previously. LSC_{214} surface decoration on the (001)-oriented LSC60-40_{113} films leads to ORR activity enhancement up to ~3 orders of magnitude with respect to bulk LSC60-40_{113}. The enhancement associated with LSC_{214} decoration for LSC60-40_{113} is similar to that reported for LSC80-20_{113}-covered LSC_{214},[5,12] where LSC_{214}-decorated LSC60-40_{113} and LSC80-20_{113} surfaces have very comparable surface oxygen exchange kinetics. Moreover, these LSC_{214}-decorated LSC60-40_{113} films (Figure 5b) have the area specific resistance approaching ~0.45 Ωcm^2 at 1 atm and 550°C, which are among the lowest reported to date.[30] While the enhancement in ORR kinetics cannot be attributed to changes in the oxygen vacancy concentration of the entire films and film strains measured at room temperature, it is proposed that interfacial LSC_{113}/LSC_{214} regions are responsible for the observed ORR enhancement. Future studies are needed to elucidate the origin of enhanced ORR kinetics at interfacial LSC_{113}/LSC_{214} regions. This study illustrates the potential of utilizing hetero-structured oxide surfaces/interfaces to develop highly active surface oxygen exchange materials for applications in the field of solid-state electrochemistry such as micro SOFC cathodes, solid-electrolyte-based sensors, and oxygen conducting membranes.

Acknowledgments

This work was supported in part by DOE (SISGR DE-SC0002633), King Abdullah University of Science and Technology, and King Fahd University of Petroleum and Minerals in Dharam, Saudi Arabia, for funding the research reported in this paper through the Center for Clean Water and Clean Energy at MIT and KFUPM. The PLD preparation performed was conducted at the Center for Nanophase Materials Sciences, which is sponsored at Oak Ridge National Laboratory by the Scientific user Facilities Division, Office of Basic Energy Sciences, U.S. Department of Energy. E. Mutoro is grateful for financial support from the German Research Foundation (DFG research scholarship). The authors thank Prof. Harry Tuller and Dr. Gerardo Jose la O' for their fruitfully discussion.

References

1. S. B. Adler, *Chem. Rev.*, **104**, 4791 (2004).
2. S. B. Adler, X. Y. Chen, and J. R. Wilson, *J. Catal.*, **245**, 91 (2007).
3. Y. L. Lee, J. Kleis, J. Rossmeisl, and D. Morgan, *Phys. Rev. B*, **80**, 20 (2009).
4. A. Tarancon, M. Burriel, J. Santiso, S. J. Skinner, and J. A. Kilner, *J. Mater. Chem.*, **20**, 3799 (2010).
5. E. J. Crumlin, E. Mutoro, S. J. Ahn, G. J. la O, D. N. Leonard, A. Borisevich, M. D. Biegalski, H. M. Christen, and Y. Shao-Horn, *J. Phys. Chem. Lett.*, **1**, 3149 (2010).
6. A. Cavallaro, M. Burriel, J. Roqueta, A. Apostolidis, A. Bernardi, A. Tarancon, R. Srinivasan, S. N. Cook, H. L. Fraser, J. A. Kilner, D. W. McComb, and J. Santiso, *Solid State Ionics*, **181**, 592 (2010).
7. W. Donner, C. Chen, M. Liu, A. J. Jacobson, Y.-L. Lee, M. Gadre, and D. Morgan, *Chem. Mater.*, **23**, 984 (2011).
8. M. Sase, F. Hermes, K. Yashiro, K. Sato, J. Mizusaki, T. Kawada, N. Sakai, and H. Yokokawa, *J. Electrochem. Soc.*, **155**, B793 (2008).
9. M. Sase, K. Yashiro, K. Sato, J. Mizusaki, T. Kawada, N. Sakai, K. Yamaji, T. Horita, and H. Yokokawa, *Solid State Ionics*, **178**, 1843 (2008).
10. N. Schichtel, C. Korte, D. Hesse, and J. Janek, *Phy. Chem. Chem. Phys.*, **11**, 3043 (2009).
11. K. Yashiro, T. Nakamura, M. Sase, F. Hermes, K. Sato, T. Kawada, and J. Mizusaki, *Electrochem. Solid State Lett.*, **12**, B135 (2009).
12. G. J. la O, S. J. Ahn, E. Crumlin, Y. Orikasa, M. D. Biegalski, H. M. Christen, and Y. Shao-Horn, *Angew. Chem. Int. Edit.*, **49**, 5344 (2010).
13. T. Kawada, K. Masuda, J. Suzuki, A. Kaimai, K. Kawamura, Y. Nigara, J. Mizusaki, H. Yugami, H. Arashi, N. Sakai, and H. Yokokawa, *Solid State Ionics*, **121**, 271 (1999).
14. A. V. Berenov, A. Atkinson, J. A. Kilner, E. Bucher, and W. Sitte, *Solid State Ionics*, **181**, 819 (2010).
15. J. Januschewsky, M. Ahrens, A. Opitz, F. Kubel, and J. Fleig, *Adv. Funct. Mater.*, **19**, 3151 (2009).
16. E. Mutoro, E. J. Crumlin, H. Pöpke, B. Luerssen, M. Amati, M. K. Abyaneh, M. D. Biegalski, H. M. Christen, L. Gregoratti, J. Janek, and Y. Shao-Horn, *J. Phys. Chem. Lett.*, **3**, 40 (2012).
17. H. J. M. Bouwmeester, H. Kruidhof, and A. J. Burggraaf, *Solid State Ionics*, **72**, 185 (1994).
18. J. Maier, *Physical Chemistry of Ionic Materials: Ions and Electrons in Solids* p. 537, John Wiley, Chichester, England; Hoboken, NJ (2004).
19. M. James, A. Tedesco, D. Cassidy, M. Colella, and P. J. Smythe, *J. Alloy Compd.*, **419**, 201 (2006).
20. M. Sánchez-Andújar and M. A. Señarís-Rodríguez, *Solid State Sci.*, **6**, 21 (2004).
21. See supplementary material at http://dx.doi.org/10.1149/2.018207jes.html for additional information.
22. T. Ishihara, T. Kudo, H. Matsuda, and Y. Takita, *J. Electrochem. Soc.*, **142**, 1519 (1995).
23. X. Y. Chen, J. S. Yu, and S. B. Adler, *Chem. Mater.*, **17**, 4537 (2005).
24. R. Sonntag, S. Neov, V. Kozhukharov, D. Neov, and J. E. ten Elshof, *Physica B*, **241**, 393 (1997).
25. H. M. Christen, E. D. Specht, S. S. Silliman, and K. S. Harshavardhan, *Phys. Rev. B*, **68**, 4 (2003).
26. G. Kim, S. Wang, A. J. Jacobson, Z. Yuan, W. Donner, C. L. Chen, L. Reimus, P. Brodersen, and C. A. Mims, *Appl. Phys. Lett.*, **88**, 3 (2006).
27. J. Maier, *Solid State Ionics*, **112**, 197 (1998).
28. L. Wang, R. Merkle, J. Maier, T. Acarturk, and U. Starke, *Appl. Phys. Lett.*, **94**, 3 (2009).
29. C. N. Munnings, S. J. Skinner, G. Amow, P. S. Whitfield, and I. J. Davidson, *Solid State Ionics*, **176**, 1895 (2005).
30. Z. P. Shao and S. M. Haile, *Nature*, **431**, 170 (2004).
31. R. A. De Souza, *Physical Chemistry Chemical Physics*, **8**, 890 (2006).
32. L. M. van der Haar, M. W. den Otter, M. Morskate, H. J. M. Bouwmeester, and H. Verweij, *J. Electrochem. Soc.*, **149**, J41 (2002).
33. R. A. De Souza and J. A. Kilner, *Solid State Ionics*, **126**, 153 (1999).
34. Y. X. Lu, C. Kreller, and S. B. Adler, *J. Electrochem. Soc.*, **156**, B513 (2009).
35. T. Kawada, J. Suzuki, M. Sase, A. Kaimai, K. Yashiro, Y. Nigara, J. Mizusaki, K. Kawamura, and H. Yugami, *J. Electrochem. Soc.*, **149**, E252 (2002).
36. W. C. Chueh and S. M. Haile, *Phys. Chem. Chem. Phys.*, **11**, 8144 (2009).
37. J. Mizusaki, Y. Mima, S. Yamauchi, K. Fueki, and H. Tagawa, *J. Solid State Chem.*, **80**, 102 (1989).
38. M. H. R. Lankhorst, H. J. M. Bouwmeester, and H. Verweij, *Phys. Rev. Lett.*, **77**, 2989 (1996).
39. M. H. R. Lankhorst, H. J. M. Bouwmeester, and H. Verweij, *J. Solid State Chem.*, **133**, 555 (1997).
40. M. H. R. Lankhorst, H. J. M. Bouwmeester, and H. Verweij, *Solid State Ionics*, **96**, 21 (1997).
41. S. Y. Wang, J. Yoon, G. Kim, D. X. Huang, H. Y. Wang, and A. J. Jacobson, *Chem. Mater.*, **22**, 776 (2010).
42. J. Suntivich, H. A. Gasteiger, N. Yabuuchi, H. Nakanishi, J. B. Goodenough, and Y. Shao-Horn, *Nature Chem.*, **3**, 647 (2011).
43. J. Suntivich, K. J. May, H. A. Gasteiger, J. B. Goodenough, and Y. Shao-Horn, *Science Express*, (2011).